

Pb-diffusion in monazite: Constraints from a high-*T* contact aureole setting

Christopher R.M. McFarlane^{a,*}, T. Mark Harrison^b

^a *Research School of Earth Sciences, Australian National University/CSIRO Exploration and Mining, Canberra, ACT 0200, Australia*

^b *Research School of Earth Sciences, Australian National University, Canberra, ACT 0200, Australia*

Received 1 February 2006; received in revised form 23 June 2006; accepted 23 June 2006

Available online 15 September 2006

Editor: C.P. Jaupart

Abstract

We report measurements of Pb diffusion in natural monazite that was subjected to a static, anhydrous, high-temperature overprint in the contact aureole of the Makhavinekh Lake Pluton (MLP), northern Labrador, Canada. The 1850 Ma monazite grains we studied were reheated to temperatures of 900 ± 25 °C during intrusion of MLP at 1322 Ma. Ion-microprobe depth-profiling reveals the outermost ~ 0.3 μm of these grains to contain Pb/U gradients that can be modeled as a result of one-dimensional concentration-independent diffusion (i.e., an error-function profile) at 1322 Ma. These gradients are combined with temperature–time histories predicted by a numerical model of conductive heat flow in the contact aureole to calculate Pb diffusion coefficients between 3.2×10^{-28} and 1.3×10^{-27} m^2/s . This range overlaps with the down-temperature extrapolation of experimental Pb diffusion data obtained under dry conditions confirming the slow diffusivity of Pb in monazite at crustal temperatures and timescales.

© 2006 Elsevier B.V. All rights reserved.

Keywords: monazite; Pb diffusion; depth-profiling; contact aureole

1. Introduction

U–Pb dating of monazite has long been used to place absolute age constraints on high-temperature crustal processes despite the fact that estimates for Pb diffusion “closure temperature” (T_c) have varied from 530 °C [1] to >1000 °C [2]. Because monazite occurs as an accessory mineral in a variety of rock types and over a range of metamorphic grades, it is also used in conjunction with U–Pb dating of zircon, rutile, and titanite

and K–Ar ages from hornblende, biotite, and feldspars to help reconstruct thermal histories of high-temperature rocks. The high-temperature portion of these paths is often dependent on our knowledge of the rate at which radiogenic Pb accumulates in monazites and zircons. However, there is a dichotomy of estimates of Pb retention in monazite, both from experimental measurements [2–4] and natural samples [5,6].

Previous attempts to constrain Pb diffusion rates in natural monazites have been hampered by uncertainties surrounding the petrogenesis of monazite relative to peak-*T* conditions [7], knowledge of heating and cooling histories [8,9], effects of armoring [10] and possible recrystallization effects in the presence of

* Corresponding author.

E-mail address: chris.mcfarlane@anu.edu.au (C.R.M. McFarlane).

hydrothermal fluids [11]. As a result, there remains a need to document Pb diffusivity in monazite under natural conditions where the temperature vs. time ($T-t$) path and a number of independent variables (e.g., P , P_{fluid} , T , dT/dt , absolute ages, and radiation doses) can be constrained with confidence. The high temperature, anhydrous contact aureole adjacent to the Makhavinekh Lake Pluton (MLP), northern Labrador is one such setting. In this communication, we use U–Pb isotopic variations, as revealed by ion microprobe depth profiling, in a monazite from this terrane to obtain a geological anchor on experimental diffusion laws [2,3].

2. The MLP aureole

The Makhavinekh Lake Pluton (MLP) is part of the Mesoproterozoic Nain Plutonic Suite of northern Labrador, northeastern Canada (Fig. 1). Details of the pluton geometry, chemistry, age, and thermal aureole have been previously described [12–17]. However, it is worthwhile reiterating several key features that make the

MLP aureole well suited to the study of Pb diffusion in monazite:

1. The MLP intruded at 1322 Ma (based on thermal ionization mass spectrometry U–Pb dates of igneous zircon) into gneissic country rocks that were regionally metamorphosed to granulite-facies at ~ 1850 Ma [16,18–22]. Thus radiogenic Pb* loss due to contact heating can be precisely resolved.
2. The diffusion-controlled coronal assemblages (e.g., symplectitic orthopyroxene + cordierite after garnet) that replaced inherited garnet in the inner aureole indicate that contact metamorphism was fluid-undersaturated and thus advective heat transport via hydrothermal fluids was likely unimportant. The morphology, composition, and age of monazite overgrowths related to contact metamorphism have also been well documented [17] enabling us to selectively avoid grains with 1322 Ma overgrowths.
3. Temperatures (at 4–5 kbar) in the aureole, calculated using robust Al-in-orthopyroxene thermometry [12], range from ~ 700 °C at 6 km distance from the pluton to

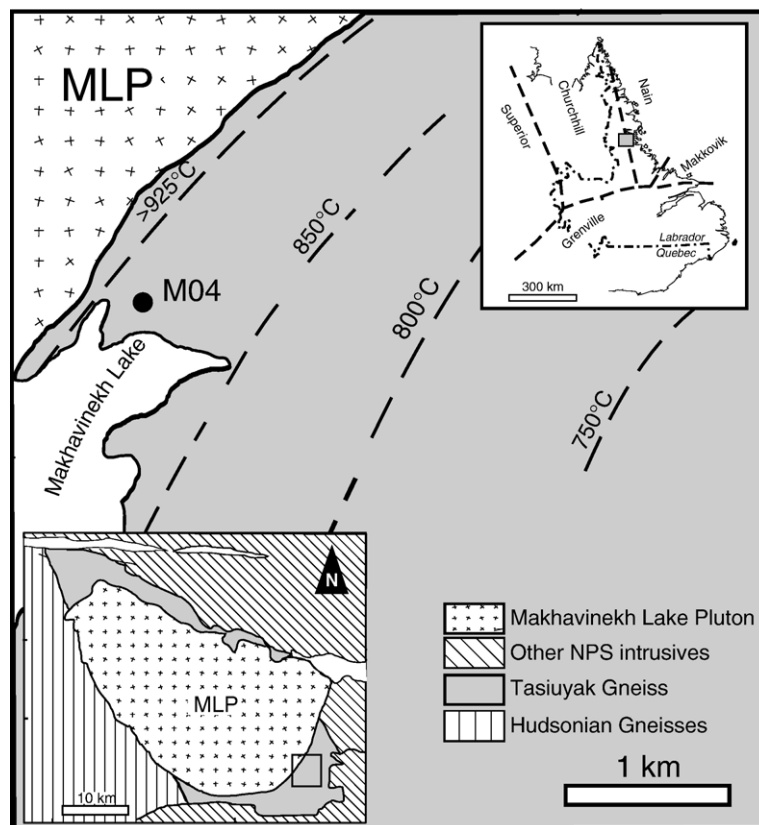


Fig. 1. Location and simplified geological map of the study area. The 1322 Ma Makhavinekh Lake Pluton (MLP) intrudes into the Tasiuyak Gneiss (paragneiss) that was metamorphosed at granulite-facies conditions at ~ 1850 Ma. Monazite was studied in sample M04 at roughly 450 m from the sub-vertical intrusive contact. Dashed lines define the peak-temperature profile moving away from the intrusion.

>925 °C at the intrusive contact (Fig. 1). These temperatures span much of the range of proposed Pb closure temperatures for monazite at geological cooling rates.

- Two-dimensional finite-difference models for conductive heat transfer in the aureole yield robust results that agree well with peak temperature estimates from 3 [11]. Thus we can use this framework to define model $T-t$ paths in the aureole.

3. Methodology

Secondary Ion Mass Spectrometry (SIMS) depth-profiles of inherited 1850 Ma monazite, separated from a sample (M04) obtained from 450 m from the MLP intrusive contact, were undertaken to document whether contact metamorphism at 1322 Ma led to measurable diffusive loss of Pb. Depth profiling was performed using a CAMECA ims 1270 ion microprobe at the University of California, Los Angeles, following the methodology outlined in similar studies [2,5]. Although we recognize that a suite of samples from different distances in the aureole would allow us to simultaneously solve for activation energy and diffusion coefficient, our primary goal here was to test the >4 order of magnitude discrepancy in diffusivity (at ~900 °C) between the available experimental datasets [2,3].

The sample was crushed and monazite separated using conventional mineral separation techniques. Monazite concentrates were hand picked to select only clear oval grains that lacked surface decorations. Grain radii (r_0) ranged from ~25 to ~75 μm . SIMS depth-profiling requires that the grains are mounted such that crystal faces are exposed to the ion beam without the need for polishing. We used a technique that employed a thin layer of acetone-soluble mounting wax to hold the grains to the mounting medium (glass slide) to ensure that they did not migrate during epoxy curing. This technique resulted in a narrow (<5 μm) ‘moat’ surrounding most unknowns but it otherwise ensured minimal surface topography on the unpolished grain mount compared to conventional doublesticky tape mounting methods. Grains were mounted with their (100) faces roughly parallel to the plane of the glass slide.

Unpolished grains were mounted along with a pre-polished standard block composed of a subset of the same clear oval monazite grains from sample M04. Polishing was sufficient to expose internal surfaces we assume are unaffected by Pb loss. Use of these grains as standard material instead of widely used monazite standards minimized potential variations in secondary ion yields resulting from mismatches in matrix composition. Although we anticipated an age uncertainty on

the order of ± 20 Ma in the standard grains, the resulting errors in the U–Pb calibration were expected to be small compared to potential age variations (e.g., up to 520 Ma) in the depth-profiles.

Standards and unknowns were analyzed using a ~3 nA primary beam and a mass resolving power sufficient to separate all molecular interferences in the 204–208 mass range (~4500). In addition to Pb and U, Au and PrPO_4^+ were also measured to monitor the removal of the Au coat and to identify when steady-state sputtering was achieved. To speed the profile acquisition (thereby increasing depth-resolution), the peak position and energy density for each mass were measured at the beginning and mid-way (i.e., after 10 blocks) through each unknown and ^{238}U measured at an energy offset of –20 V relative to the Pb masses. Typical 1σ analytical errors on $^{207}\text{Pb}/^{235}\text{U}$ and $^{206}\text{Pb}/^{238}\text{U}$ measurements for polished standards were 2–3%. Examination of the standard analyses revealed a systematic time-dependent drift in Pb/U vs. UO/U away from the typical calibration slope for the Cameca ims1270. During the analysis of unknowns, this down-hole fractionation had the effect of dispersing data measured early in the acquisition towards normal discordance, whereas data collected later became reversely discordant. A secondary normalization to compensate for this down-hole fractionation was, therefore, applied offline to standards and unknowns. This involved calculating three separate U–Pb calibrations for intervals of ca. 200s each (i.e., minimum of four analytical blocks) moving down the sputter pit (see Fig. 2A). This approach yielded tight clusters of concordant standard ages of 1841 ± 45 Ma, 1844 ± 16 Ma, and 1857 ± 27 Ma, respectively (see Fig. 2A) for the three independent calibrations which were applied to the unknowns over the same time intervals. This correction scheme effectively removed the bulk of the anomalous discordance in the unknown profiles (see Fig. 2B) allowing us to calculate diffusion coefficients with greater confidence.

Once the standards and unknowns were analyzed, the depth of the sputter pits produced during standard analyzes were measured using a DekTak™ surface profilometer with nominal error of ± 0.005 μm allowing us to calculate an average sputter rate of ~0.2 nm/s. Weighted mean profiles and linear regressions were performed using Isoplot 3.00 [23].

4. Results

Depth profiling revealed smoothly increasing $^{206}\text{Pb}^*/^{238}\text{U}$ and $^{207}\text{Pb}^*/^{235}\text{U}$ dates from over the outermost ~0.3 μm of the grains. Fig. 2B shows the corrected

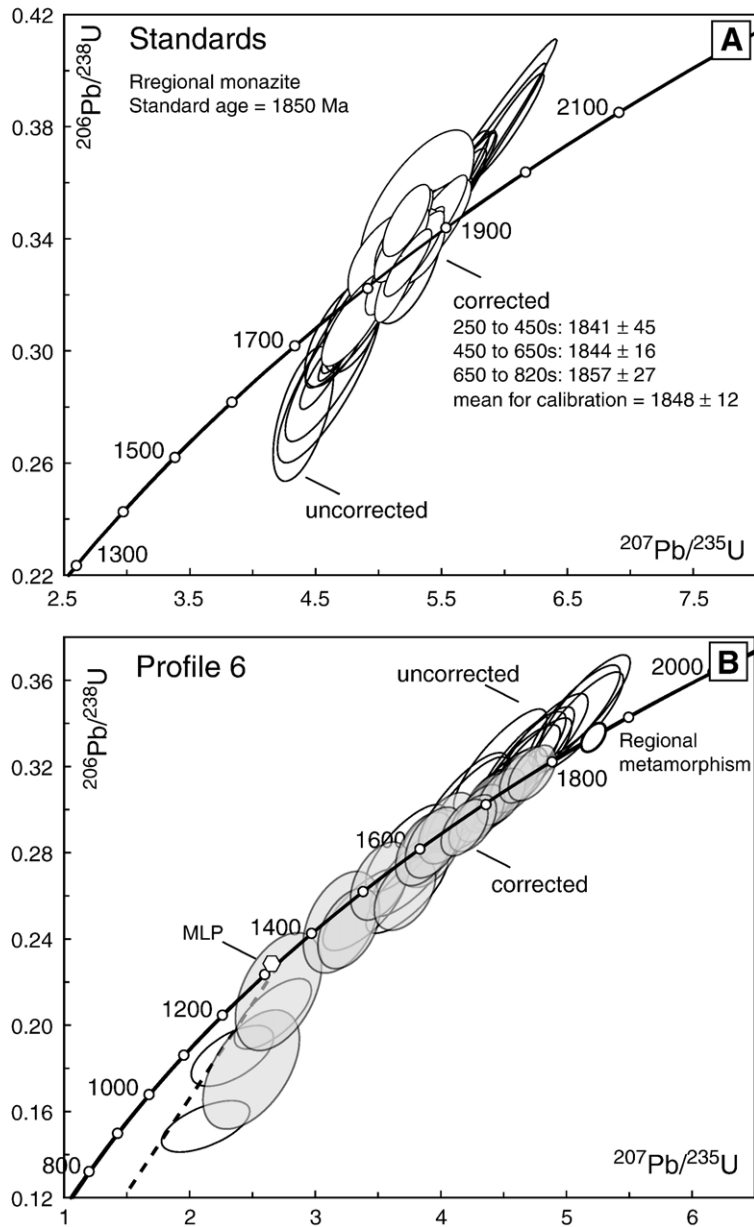


Fig. 2. Conventional Concordia diagrams for standards and unknowns. (A) Data for standard analyses of pre-polished 1850 Ma monazite grains. Uncorrected data (open ellipses) are dispersed along a line between ~ 1850 Ma and 0 Ma as a result of down-hole fractionation of Pb/U. Data corrected using the method outlined in the text (filled ellipses) are concordant at ~ 1850 Ma for each time (depth) interval. (B) Uncorrected vs. corrected data for a single unknown profile. Uncorrected data (open ellipses) are systematically normally discordant at the start of the profile, and reversely discordant at the end of the profile. Corrected data define a near-concordant array between 1800 Ma and 1300 Ma, consistent with diffusive Pb-loss in regional monazite during contact heating. Normally discordant data in the first two blocks appear to have experienced recent Pb-loss, and parallel a chord (dashed line) anchored between 1322 and 0 Ma.

and uncorrected U–Pb data for a single unknown profile and demonstrates the veracity of the fractionation correction applied to the depth-profile data. The corrected profile (shaded ellipses) defines an array of near-concordant points (1σ errors) between ~ 1800 Ma

and ~ 1300 Ma. The outermost two blocks of the corrected profile (i.e., two youngest data points) deviate from this array and plot below Concordia, roughly parallel to a chord (dashed line) anchored between 1322 and 0 Ma.

Fig. 3 shows the weighted mean Pb*/U age profiles (2σ errors) based on four fractionation-corrected unpolished unknowns. The dashed line shows the percentage of radiogenic ^{206}Pb ($^{206}\text{Pb}^*$) moving deeper into the grains. In all the unpolished grains examined, removal of the Au coating and significant common-Pb contamination was typically complete after three analysis blocks. Excluding the first two blocks in Fig. 3, the profile displays a smooth increase in Pb*/U ages from ~ 1300 Ma at a depth of $0.06\ \mu\text{m}$ to ~ 1800 Ma at a depth of $0.30\ \mu\text{m}$. The intensity of U for these profiles decrease with depth in manner similar to the polished standard material. Although several other profiles were encountered, most were discarded because they displayed anomalously high common-Pb concentrations over the outermost half of the profiles (e.g., intersected a microfracture). In other cases, a slight tilt on the unpolished grain caused the ion-beam to intersect the surface at an angle (as revealed using the

profilometer) giving rise to anomalously shallow Pb*/U profiles.

5. Discussion

If the 1850 Ma monazite grains had lost radiogenic Pb exclusively by Pb-diffusion due to intrusion of the MLP, we would expect the outermost portion of each profile to record ages of ~ 1320 Ma. Although the first one to two blocks shown in Figs. 2B and 3 fall below this age, the higher concentration of common-Pb in these analyses (up to 15%) suggests that the outermost 50 nm of the grains has been affected by recent Pb-loss (e.g., interaction with low-temperature meteoric fluids). Excluding these points, the profiles shown in Figs. 2 and 3 are consistent with our model for high-temperature Pb-diffusion in inherited 1850 Ma during intrusion of the MLP at 1322 Ma.

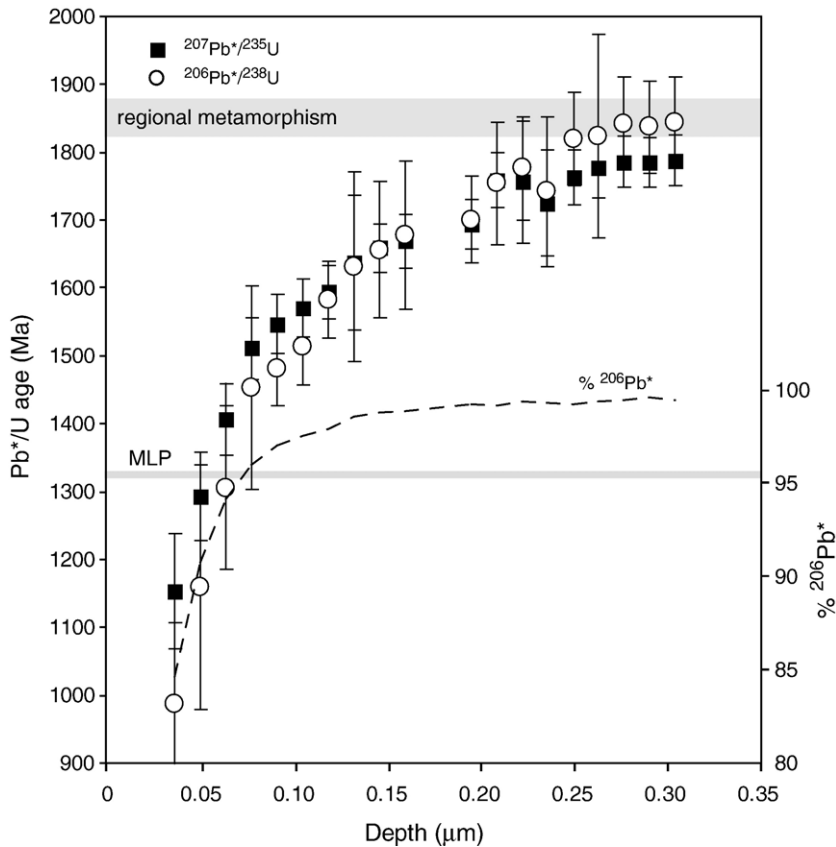


Fig. 3. Corrected $^{206}\text{Pb}^*/^{238}\text{U}$ (open circles) and $^{207}\text{Pb}^*/^{235}\text{U}$ (closed squares) dates vs. depth for unpolished monazite grains ($n=4$) from 450 m from the MLP intrusion (sample M04). Grey horizontal lines show the ages of inherited (regional metamorphic) monazite (1850 ± 20 Ma) components and the timing of contact metamorphism during intrusion of the MLP (1322 Ma). The dashed line shows the calculated percentage of radiogenic ^{206}Pb encountered as a function of depth. The gap in data between 0.16 and $0.19\ \mu\text{m}$ is the result of peak-centering mid-way through the acquisition. Ages significantly younger than 1322 Ma in the outermost two blocks (with the highest common-Pb content) are interpreted to reflect recent Pb-loss.

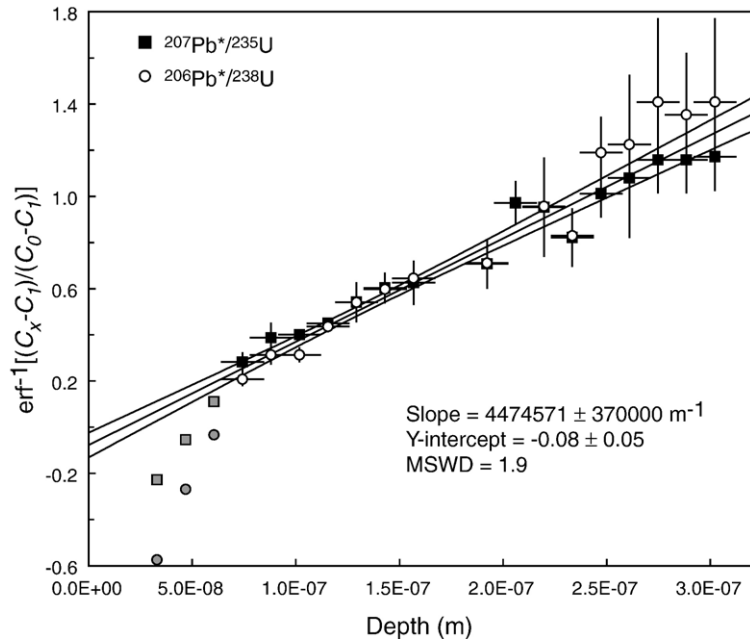


Fig. 4. Normalized concentration gradients for the $^{207}\text{Pb}^*/^{235}\text{U}$ and $^{206}\text{Pb}^*/^{238}\text{U}$ profiles (2σ error bars) inverted through the error function (symbols as in Fig. 2). Concentrations at each depth (C_x) have been normalized assuming an inherited concentration equivalent to 1850 Ma (C_0) and a boundary concentration equivalent to 1322 Ma (C_1). The combined Pb*/U profile defines a regression of slope $(4Dt)^{-1/2}$. Convergence of the calculated regression line at a Y-intercept of 0 is predicted if diffusion occurred at 1322 Ma. Grey symbols are data from the outermost region of the grains that display evidence for recent Pb-loss and were excluded from the regression calculation.

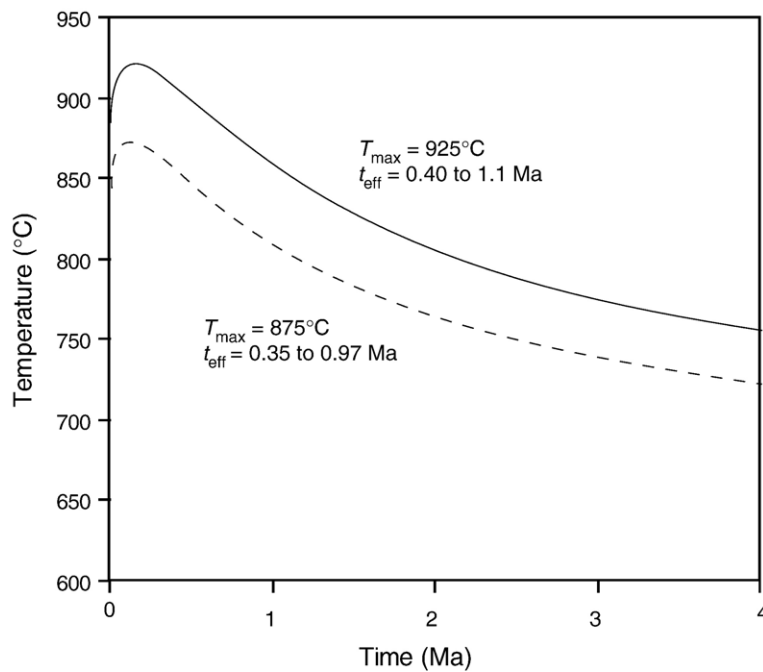


Fig. 5. Model temperature–time paths at a distance of 450 m from the MLP generated using a numerical two-dimensional finite-difference method solution to the conductive heat transfer equation. The upper and lower $T-t$ paths bound the range of the estimated peak temperature for sample M04 (900 ± 25 °C). The range of effective timescales for diffusion (T_{eff}) for each path was calculated from experimentally determined activation energies and diffusion coefficients for Pb diffusion [2,4].

5.1. Testing for Pb diffusion at 1322 Ma

We can test whether the observed age gradients resulted from Pb diffusion (as opposed to a non-Fickian transport mechanism) at 1322 Ma by recasting the U–Pb ages in terms of concentration as a function of depth (C_x) [2,4]. Rather than attempt to fit error functions directly to the profile, we chose to invert the concentration information through the error function (erf^{-1}) and use the expectation of linearity to confirm the preservation of diffusion-controlled profiles produced at 1322 Ma.

Fig. 4 is a plot of $\text{erf}^{-1}[(C_x - C_1)/(C_0 - C_1)]$ vs. depth for the measured $^{207}\text{Pb}^*/^{235}\text{U}$ and $^{206}\text{Pb}^*/^{238}\text{U}$ profiles assuming an unaffected interior concentration (C_0) equivalent to 1850 Ma and a boundary concentration (C_1) equivalent to 1322 Ma. If the concentration profiles resulted exclusively from Pb diffusion at 1322 Ma, the data should plot as a line passing through the origin with

a slope of $(4Dt)^{-1/2}$. A line regressed through all but the first three data points (which display a significant common-Pb component) yields a slope of $4.47 \pm 0.37 \times 10^6 \text{ m}^{-1}$ with an essentially zero intercept (i.e., -0.08 ± 0.05 ; MSWD=1.9).

5.2. T - t paths

In order to calculate a Pb diffusion coefficient from these data, we require an estimate of the timescale of the thermal perturbation that affected the inherited monazite grains during intrusion of the MLP. Although the age profiles shown in Figs. 2 and 3 must be the result of Pb diffusion integrated over the duration of the thermal pulse, the bulk of the diffusion occurs close to the maximum temperature (T_{max}) achieved along the T - t path. We have, therefore, calculated an apparent, or effective timescale (τ) [24] that the sample spent at T_{max} . This approach requires us to use explicit values for

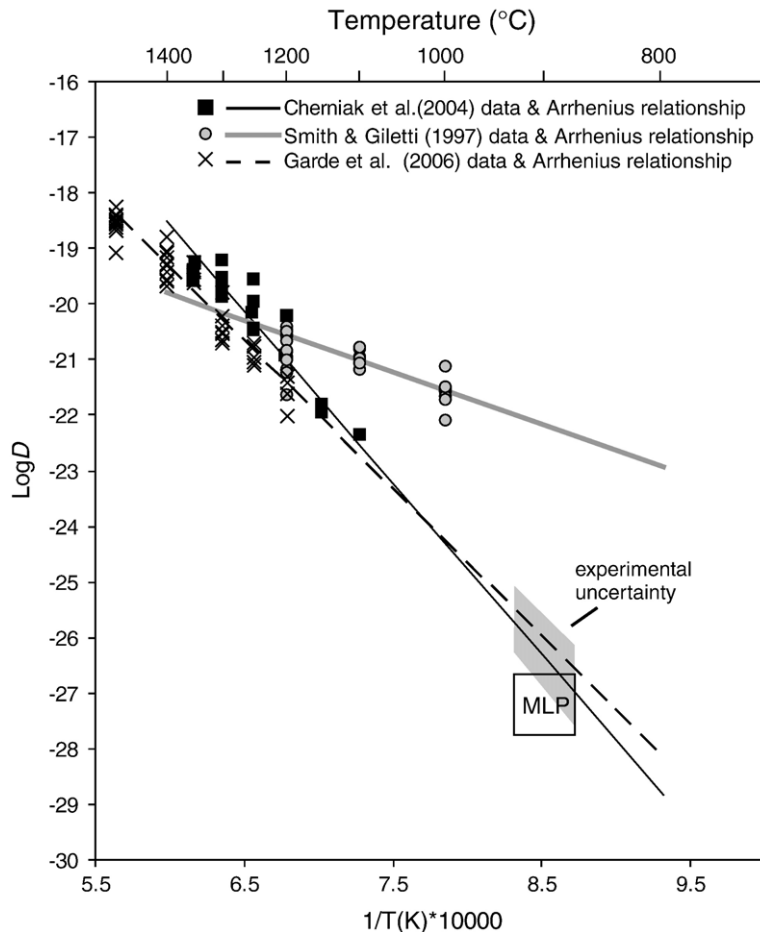


Fig. 6. Arrhenius plot showing the Pb diffusion estimate from the MLP relative to experimentally derived diffusion laws. The shaded polygon shows the uncertainty on experimental data extrapolated to 900 °C. Our estimate overlaps with the down-temperature extrapolation of [2] and [3].

activation (E_a) and frequency factor (D_0) in order to calculate $D(T, t)$ at each point along the $T-t$ path assuming Arrhenius temperature dependence. Effective timescales ($\tau = \sum_0^t D\Delta t/D_{\max}$) were calculated for the range of E_a (592–180 kJ/mol) and D_0 ($0.94-6.61 \times 10^{-15} \text{ m}^2/\text{s}$) obtained experimentally [2,4].

Assuming heat transfer in the aureole was characterized by conduction, $T-t$ paths at 450 m can be modeled using either a one-dimensional analytical solution or a two dimensional finite-difference method approach [25,26]. In either case, the models must satisfy independent constraints for the peak temperature of $900 \pm 25 \text{ }^\circ\text{C}$ at 450 m (based on robust Al-solubility thermometry) from the intrusive contact and for the characteristic cooling time ($t = r^2/k$, where k is thermal diffusivity) of $\sim 8 \text{ Ma}$ for a pluton of radius of 16 km [27]. The $T-t$ profiles used here are modeled using a two-dimensional numerical finite-difference algorithm described in previous studies of the MLP aureole [12,28] using a value of Δt of 5 ka. Input variables (e.g., intrusion temperature, geothermal gradient, thermal diffusivity) were chosen to produce $T-t$ paths that achieved peak temperatures of $\sim 925 \text{ }^\circ\text{C}$ and $\sim 875 \text{ }^\circ\text{C}$ at a distance of 450 m from the vertical intrusive contact (Fig. 5). These $T-t$ paths span a range of effective timescales between 0.35 Ma for $T_{\max} = 875 \text{ }^\circ\text{C}$ and 1.1 Ma for $T_{\max} = 925 \text{ }^\circ\text{C}$.

5.3. Pb-diffusion estimates

Combining this range of effective timescales with the slopes derived from the erf^{-1} plot shown in Fig. 4 yields a range of D values between 3.2×10^{-28} and $1.3 \times 10^{-27} \text{ m}^2/\text{s}$. This datum is shown in Fig. 6 relative to experimentally derived Arrhenius relationships for Pb diffusion in monazite [2–4].

Our results are consistent with the down-temperature extrapolation of the experimental results of [2] and [3], confirming the very low diffusivity of Pb in monazite under anhydrous conditions. It remains possible that the difference between more recent anhydrous experiments and those of Smith and Giletti [4] reflect a water-pressure dependence on the diffusion of Pb in monazite. We note, however, that no such effect has been previously observed for cation diffusion in silicates [29] or phosphates [30,31].

We conclude that volume diffusion of Pb* is unlikely to cause grain-scale resetting of the U–Pb system in monazite under normal crustal conditions. In cases where resetting can be demonstrated to have affected monazite at the grain scale [6], we suggest that recrystallization mechanisms should be investigated, especial-

ly in rocks where hydrous alteration has affected the major-mineral assemblage (e.g., pinnitized cordierite or chloritized garnet) and where gradients in Pb are accompanied by variations in Ca, Y, and U [11].

Acknowledgements

This work was funded by Australian Research Council Discovery Project DP0558217 to C.R.M. McFarlane. Many thanks to Marty Grove for ion-microprobe assistance and to Peter Collett for his keen eyes and patient picking. Thanks also to Trevor Ireland for his ion-probe insights. The manuscript benefited from the input of two anonymous reviewers. The ion microprobe facility at UCLA is partly supported by a grant from the Instrumentation and Facilities Program, Division of Earth Sciences, National Science Foundation.

References

- [1] L.P. Black, J.D. Fitzgerald, S.L. Harley, Pb isotopic composition, colour and microstructure of monazites from a polymetamorphic rock in Antarctica, *Contrib. Mineral. Petrol.* 85 (1984) 141–148.
- [2] D.J. Cherniak, B.E. Watson, M. Grove, T.M. Harrison, Pb diffusion in monazite: a combined RBS/SIMS study, *Geochim. Cosmochim. Acta* 68 (2004) 829–840.
- [3] E. Gardé, O. Jaoul, J.M. Montel, A.M. Seydoux-Guillaume, R. Wirth, Pb diffusion in monazite: An experimental study of $\text{Pb}^{2+} + \text{Th}^{4+} \leftrightarrow 2\text{Nd}^{3+}$ interdiffusion, *Geochim. Cosmochim. Acta* 70 (2006) 2325–2336.
- [4] H.A. Smith, B.J. Giletti, Lead diffusion in monazite, *Geochim. Cosmochim. Acta* 61 (1997) 1047–1055.
- [5] M. Grove, T.M. Harrison, Monazite Th–Pb age depth profiling, *Geology* 27 (1999) 487–490.
- [6] K. Suzuki, M. Adachi, I. Kajizuka, Electron microprobe observations of Pb diffusion in metamorphosed detrital monazites, *Earth Planet. Sci. Lett.* 128 (1994) 391–405.
- [7] B. Bingen, O. Van Breemen, U–Pb monazite ages in amphibolite- to granulite facies orthogneiss reflect hydrous mineral breakdown reactions: Sveconorwegian Province of SW Norway, *Contrib. Mineral. Petrol.* 132 (1998) 336–353.
- [8] F.S. Spear, R. Parrish, Petrology and cooling rates of the Valhalla Complex, British Columbia, Canada, *J. Petrol.* 37 (1996) 733–765.
- [9] D. Bosch, D. Hammor, O. Bruguier, R. Caby, J.-M. Luck, Monazite “in situ” $^{207}\text{Pb}/^{206}\text{Pb}$ geochronology using a small geometry high-resolution ion probe. Application to Archean and Proterozoic rocks, *Chem. Geol.* 184 (2002) 151–165.
- [10] J.M. Montel, D. Kornprobst, D. Vielzeuf, Preservation of old U–Th–Pb ages in shielded monazite: example from the Beni Bousera Hercynian kinzigites (Morocco), *J. Metamorph. Geol.* 18 (2000) 335–342.
- [11] A.M. Seydoux-Guillaume, J.L. Paquette, M. Wiedenbeck, J.M. Montel, W. Heinrich, Experimental resetting of the U–Th–Pb systems in monazite, *Chem. Geol.* 191 (2002) 165–181.
- [12] C.R.M. McFarlane, W.D. Carlson, J.N. Connelly, Prograde, peak, and retrograde P–T paths from aluminium in orthopyroxene: High-temperature contact metamorphism in the aureole

- of the Makhavinekh Lake Pluton, Nain Plutonic Suite, Labrador, *J. Metamorph. Geol.* 21 (2003) 405–423.
- [13] B. Ryan, Makhavinekh lake pluton, Labrador, Canada: geological setting, subdivisions, mode of emplacement, and a comparison with Finnish rapakivi granites, *Precambrian Res.* 51 (1991) 193–225.
- [14] Y. Yang, S.A. Morse, $^{40}\text{Ar}/^{39}\text{Ar}$ chronology of the Nain anorthosites, Canada, *Can. J. Earth Sci.* 30 (1993) 1166–1178.
- [15] J.H. Berg, Dry granulites mineral assemblages in the contact aureoles of the Nain Complex, Labrador, *Contrib. Mineral. Petrol.* 64 (1977) 33–52.
- [16] C.R.M. McFarlane, J.N. Connelly, W.D. Carlson, Intracrystalline redistribution of Pb in zircon during high-temperature contact metamorphism, *Chem. Geol.* 217 (2005) 1–28.
- [17] C.R.M. McFarlane, J.N. Connelly, W.D. Carlson, Monazite and xenotime petrogenesis in the contact aureole of the Makhavinekh Lake Pluton, northern Labrador, *Contrib. Mineral. Petrol.* 148 (2005) 524–541.
- [18] J.M. Bertrand, M. Van Kranendonk, S. Hanmer, J.C. Roddick, I. Ermanovics, Structural and metamorphic geochronology of the Torngat Orogen in the North River-Nutak transect area, Labrador: preliminary results of U–Pb dating, *Geosci. Can.* 17 (1991) 297–301.
- [19] J.M. Bertrand, J.C. Roddick, K.M.J. Van, I. Ermanovics, U–Pb geochronology of deformation and metamorphism across a central transect of the early Proterozoic Torngat Orogen, North River map area, Labrador, *Can. J. Earth Sci.* 30 (1993) 1470–1489.
- [20] F. Mengel, T. Rivers, Metamorphism in the Paleoproterozoic Torngat Orogen, Labrador: Petrology and P–T–t paths of amphibolite- and granulite-facies rocks across the Komaktorvik shear zone, *Can. Mineral.* 35 (1997) 1137–1160.
- [21] D.J. Scott, An overview of the U–Pb geochronology of the Paleoproterozoic Torngat Orogen, Northeastern Canada, *Precambrian Res.* 91 (1998) 91–107.
- [22] M.J. Van Kranendonk, Geological evolution of the Archean Nain province and the early Proterozoic Torngat Orogen as seen along a transect in the North River- Nutak map area, northern Labrador, Canada, Doctoral, Queen’s University, 1992.
- [23] K.R. Ludwig, *Isoplot 3.00: A Geochronological Toolkit for Microsoft Excel*, Berkeley, Geochronological Centre Special Publication, vol. 4, 2003.
- [24] T.M. Harrison, I. McDougall, Investigations of an intrusive contact, northwest Nelson, New Zealand- II. Diffusion of radiogenic and excess ^{40}Ar in hornblende revealed by $^{40}\text{Ar}/^{39}\text{Ar}$ age spectrum analysis, *Geochim. Cosmochim. Acta* 44 (1980) 2005–2020.
- [25] J. Alcock, K. Myer, P.D. Muller, Three-dimensional model of heat flow in the aureole of the Marcy Anorthosite, Adirondack Highlands, New York: implications for depth of emplacement, *Geol. Mat. Res.* 1 (1999) 1–21.
- [26] J.R. Bowers, D.M. Kerrick, K.P. Furlong, Conduction model for the thermal evolution of the Cupsuptic aureole, Maine, *Am. J. Sci.* 290 (1990) 644–664.
- [27] J.C. Jaeger, Thermal effects of intrusions, *Rev. Geophys.* 2 (1964) 443–466.
- [28] W.D. Carlson, Rates of Fe, Mg, Mn, and Ca diffusion in garnet, *Am. Mineral.* 91 (2006) 1–11.
- [29] D.J. Cherniak, E.B. Watson, Pb diffusion in zircon, *Chem. Geol.* 172 (2000) 5–24.
- [30] D.J. Cherniak, F.J. Ryerson, A study of strontium diffusion in apatite using Rutherford Backscattering and ion implantation, *Geochim. Cosmochim. Acta* 57 (1993) 4653–4662.
- [31] J.R. Farver, B.J. Giletti, Strontium diffusion kinetics in apatite, *Eos, Trans. - Am. Geophys. Union* 79 (1998) 369.